Electronic Supplementary Material (ESI) for Nanoscale.
This journal is © The Royal Society of Chemistry 2022

Supplementary Information

Computational hyperspectral devices based on quasi-random metasurface supercells

Cong Chen,[a,c] Xiaoyin Li,[b] Gang Yang,[b,d] Xiaohu Chen,[c] Hui Li,[a,c] Yinghui Guo[b,d]* and Shoupeng Liu[a,c]*

[a] *School of Biomedical Engineering (Suzhou), Division of Life Science and Medicine, University of Science and Technology of China, Suzhou 215163, China*

[b] *State Key Laboratory of Optical Technologies on Nano-Fabrication and Micro-Engineering, Institute of Optics and Electronics, Chinese Academy of Sciences, Chengdu 610209, China*

[c] *Suzhou Institute of Biomedical Engineering and Technology, Chinese Academy of Sciences, Suzhou 215163, China*

[d] *University of Chinese Academy of Sciences, School of Optoelectronics, Beijing 100049, China*

*Correspondence: (Y. G) gyh@ioe.ac.cn; (S. L) liusp@sibet.ac.cn

Part 1: Principle of the spectral reconstruction algorithm.

According to Eq. (1) of this study, the compressive sensing algorithm based on sparse optimization and dictionary learning [1,2] has been used to reconstruct the incident spectral signal. A sparse incident signal is an essential prerequisite for realizing compressed sensing is the sparse incident signal. However, since most spectra are not sparse in natural environments, the incident spectral signals need to be sparsely processed and represented as follows:

$$f=\Psi s \tag{S1}$$

where, f represents an incident spectrum. Ψ and s represent the sparse basis matrix and sparse coefficient, respectively. Thus, Eq. (1) can be rewritten as follows:

$$I=T\Psi s \tag{S2}$$

where I and T represent the observation signal and observation matrix of the compressive sensing algorithm, respectively. Based on Eq. (S2), the problem of solving the incident signal can be converted into the l_1 norm as follows:

$$\min\|s\|_1 \quad \text{s.t.} \quad \|f\Psi s-I\|_2 \le \delta \tag{S3}$$

$$\|s\|_1=\sum_{j=1}^{m} f_j \tag{S4}$$

where, δ represents a positive constant. The optimal solution s for Eq. (S3) and Eq. (S4) can be obtained simultaneously. The incident spectrum f can be calculated according to Eq. (S1). Presently, many algorithms for solving the original signal based on the given principle.[3] The orthogonal matching pursuit (OMP) algorithm has been used to reconstruct the spectral signal in this work due to its high optimization efficiency. The pseudo-code of OMP is given as follows:

(1) Input: $y=T*f$, $A=T*\Psi$, sparsity = k;
(2) Initialization: residual $r=y$, define two empty matrices (AA and PP);
(3) Computation: [val, pos]=max($A^{T}*r$), $AA_i=[AA_{i-1},A(:,\text{pos})]$, $PP_i=[PP_{i-1},\text{pos}]$, $X=(AA^{T}*AA)^{-1}*A^{T}*r$;
(4) Update residual: $r=y-AA*X$;
(5) Judgment: $i=i+1$, if $i<k$, return to step (3);
(6) Output: reconstructed original signal $f'=\Psi*X$.

Part2: Metasurface fabrication

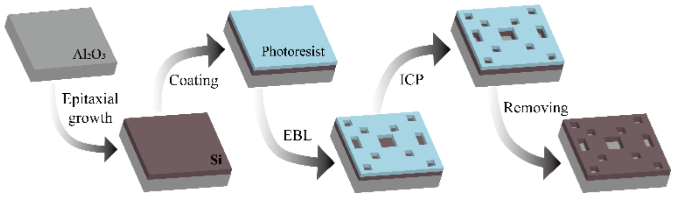

Fig. S1 The fabrication process of the samples

A 200 nm Si film was epitaxially grown on the Al_2O_3 substrate. Then, an electron beam photoresist was spin-coated on the Si film. Next, a quasi-random metasurface supercell array pattern was displayed on the photoresist using electron beam lithography (EBL), which was transferred onto the Si film by inductively coupled plasma (ICP). Finally, the photoresist is removed, completing the processing of the samples.

Part 3: Schematic representation of quasi-random metasurface supercells selected by the optimization algorithm.

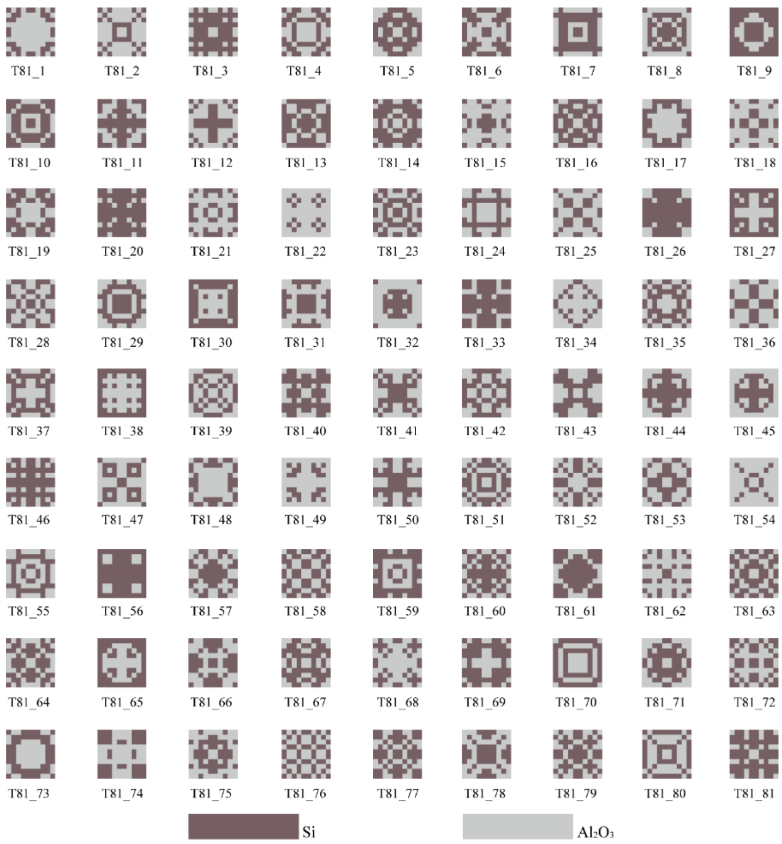

Fig. S2 The top views of the 81 quasi-random metasurface supercells selected by the optimization algorithm.

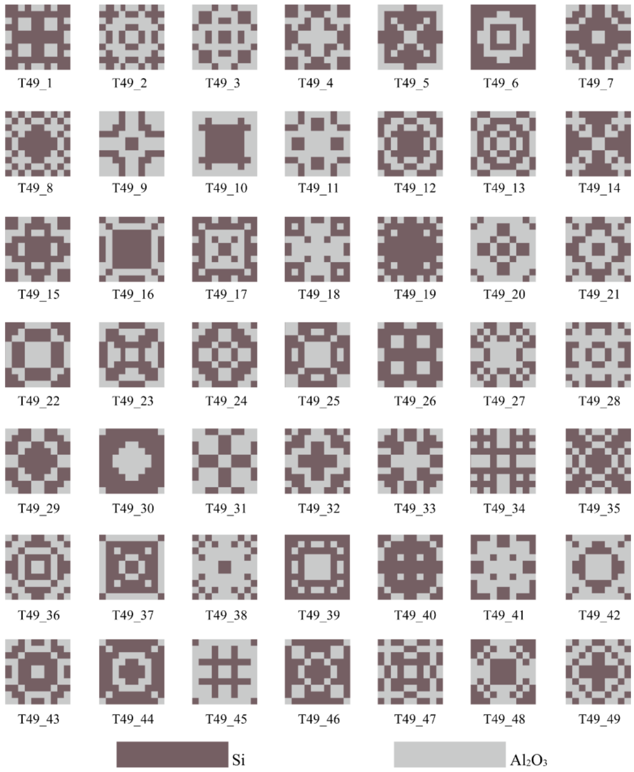

Fig. S3 The top views of the 49 quasi-random metasurface supercells selected by the optimization algorithm.

Part 4: Simulation results of the metasurface supercells.

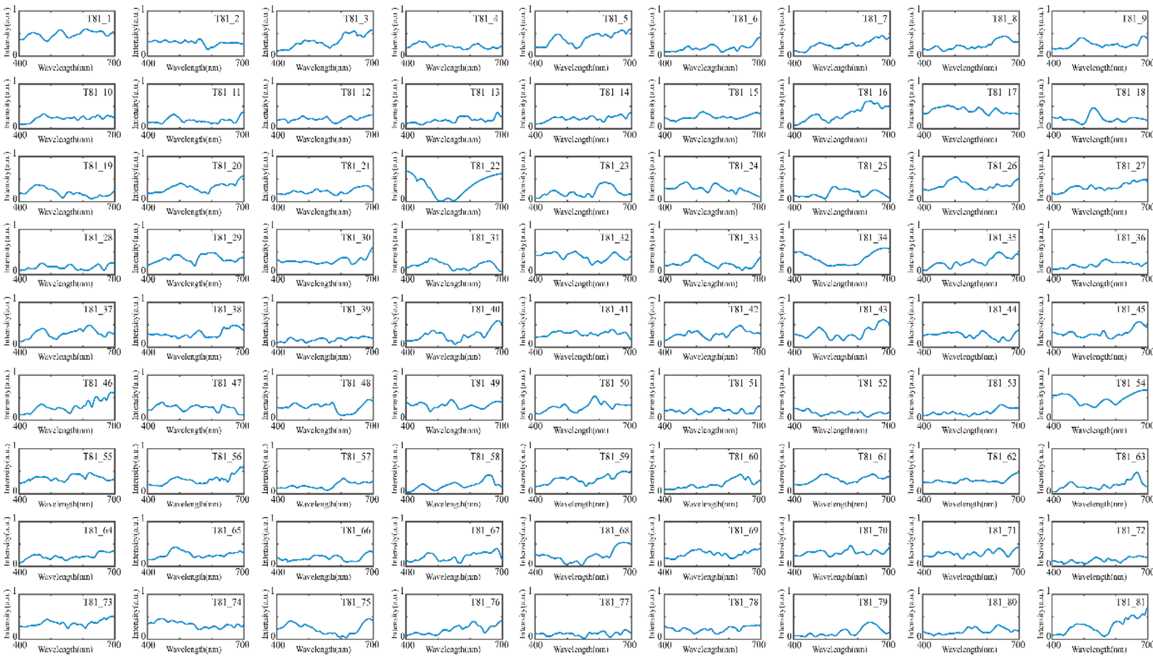

Fig. S4. Transmission spectra obtained by the simulation of the metasurface supercells shown in Fig. S1.

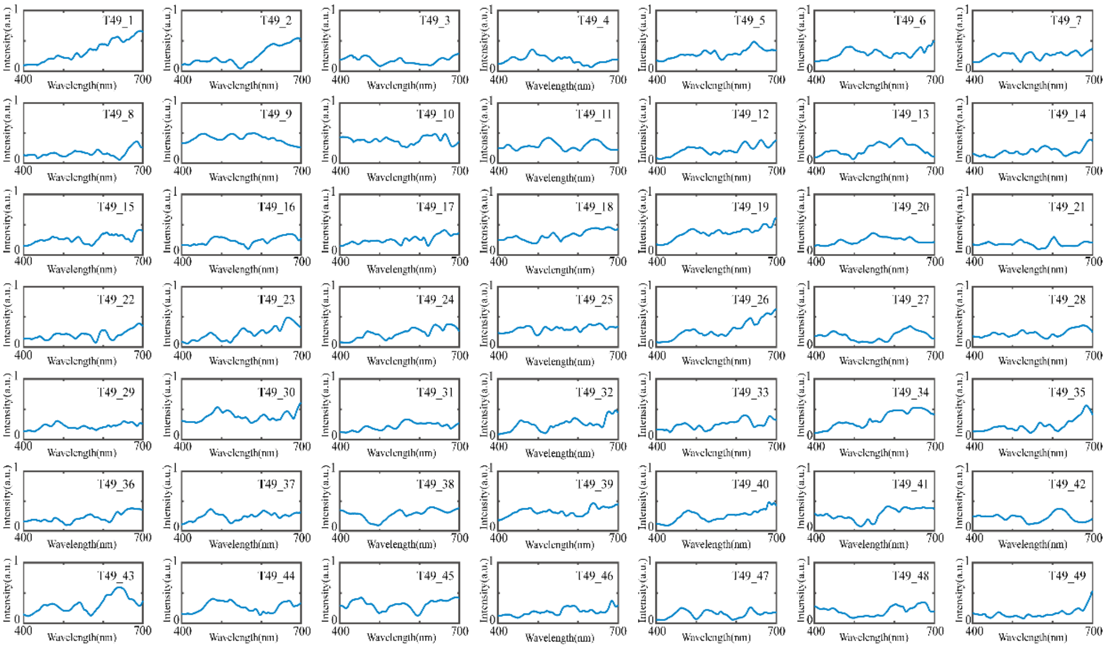

Fig. S5. Transmission spectra obtained by the simulation of the metasurface supercells shown in Fig. S2.

Part 5: Simulation results of the metasurface cells for a previously reported study.

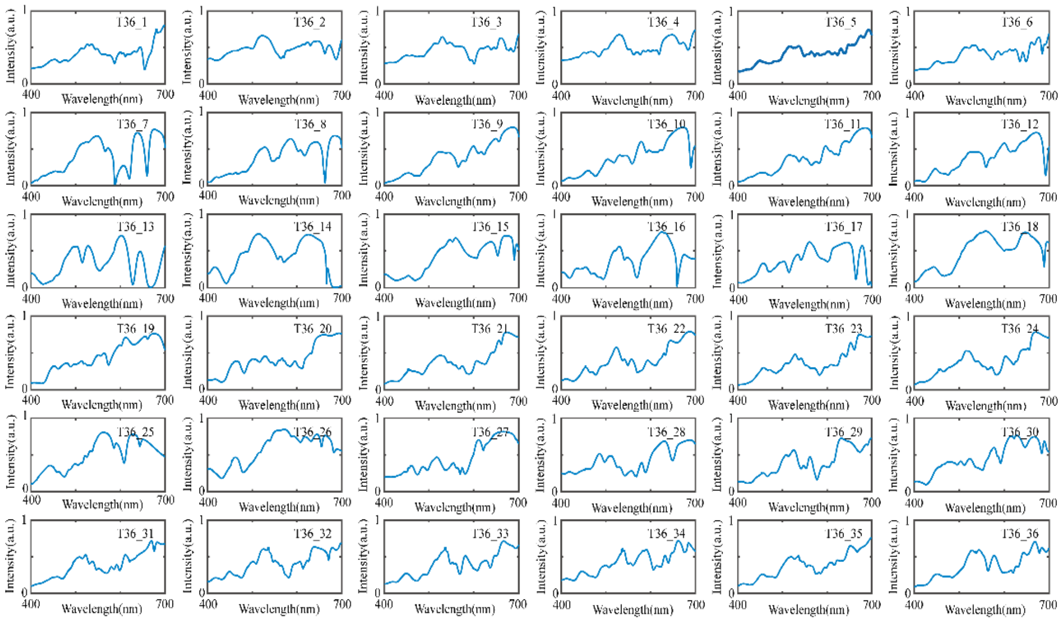

Fig. S6 Transmission spectra obtained by the simulation of 36 metasurface cells for a previously reported study.[4] The geometric parameters of the metasurface cells as per the referred study.[4] The simulation conditions and materials are consistent with those given in part 2.

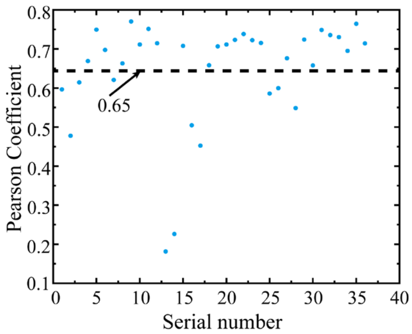

Fig. S7 Pearson's correlation coefficient of the 36 transmission spectra shown in Fig. S5. The black dotted line is the average values of Pearson's correlation coefficients.

Part 6: Simulation results of the complex narrowband spectral reconstruction.

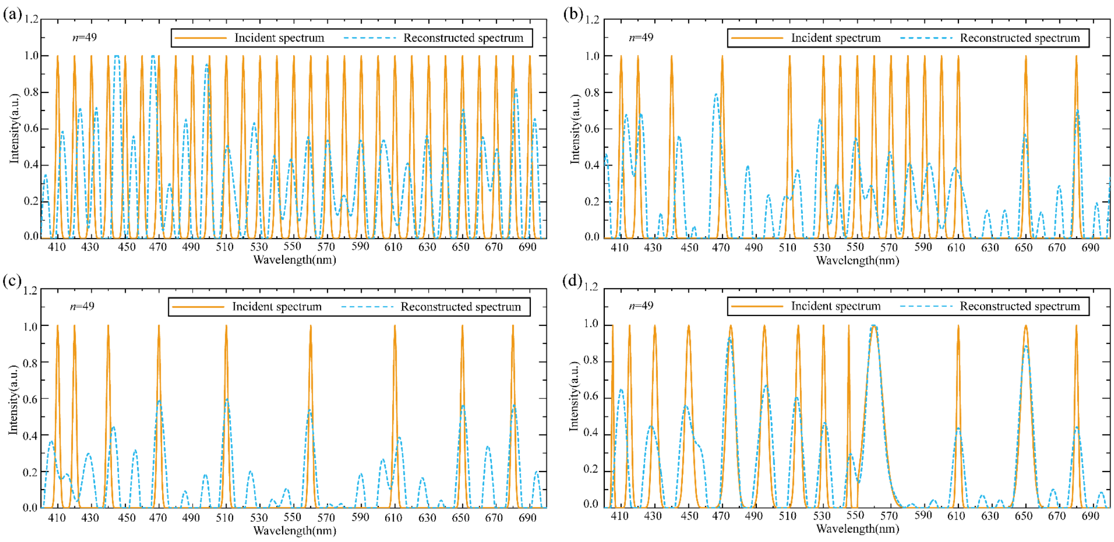

Fig. S8 Simulation results of narrowband spectrum reconstructed by the CHDBS consists of 49 metasurface supercells (*n*=49). The incident spectra in (a), (b), (c), and (d) correspond to the incident spectra given in Figs. 4(a), (f), (g), and (h), respectively.

Part 7: Experimental results of the metasurface supercell arrays.

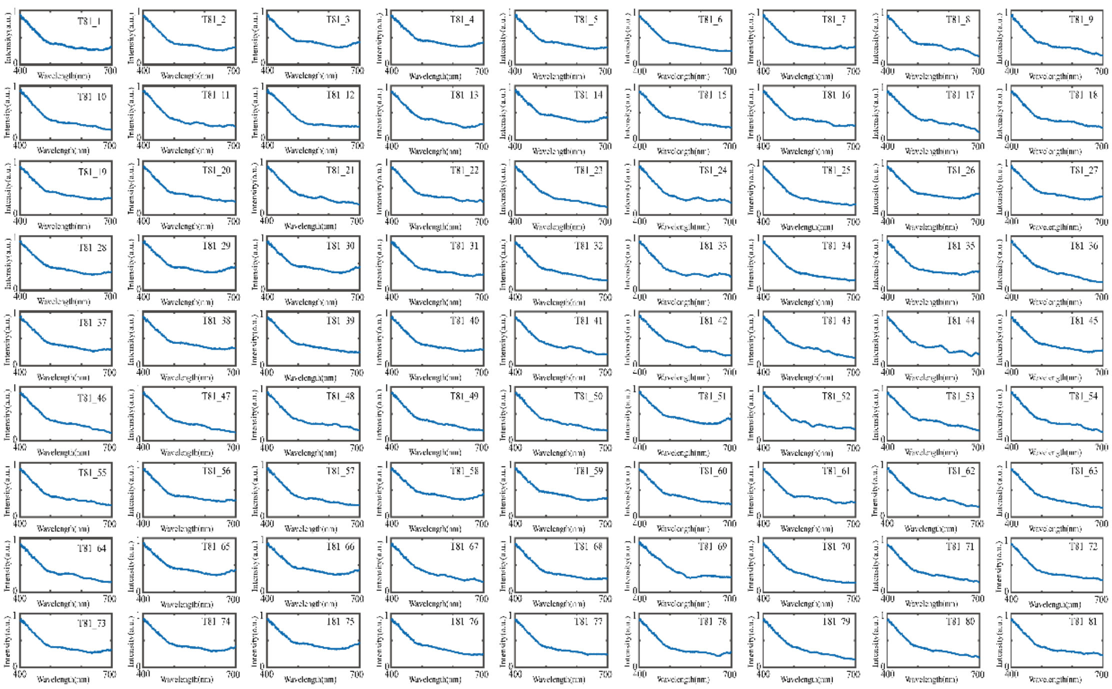

Fig. S9 Experimentally measured transmission spectra of the metasurface supercells shown in Fig. S1.

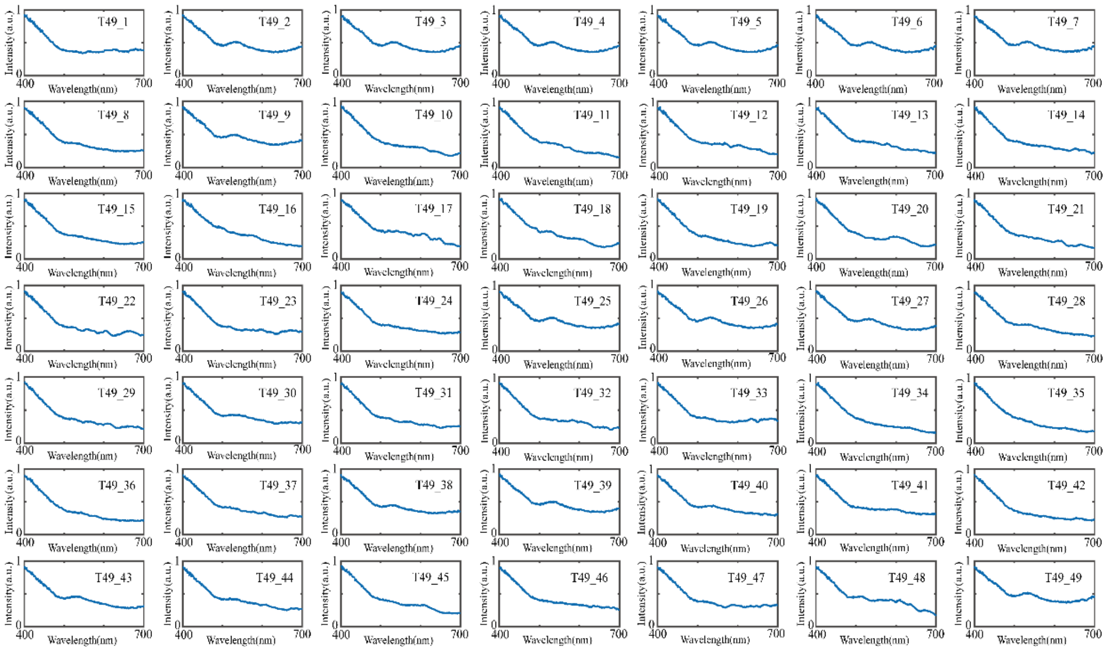

Fig. S10 Experimentally measured transmission spectra of the metasurface supercells shown in Fig. S2.

References

1. C.-C. Chang, N.-T. Lin, U. Kurokawa and C. Byung II, Optical Engineering, 2012, **51**, 059804.

2. S. Zhang, Y. Dong, H. Fu, S.-L. Huang and L. Zhang, Sensors, 2018, **18**, 644.

3. J. A. Tropp, S. J. Wright. Proceedings of the IEEE, 2010, **98**, 948-958.

4. J. Xiong, X. Cai, K. Cui, Y. Huang, J. Yang, H. Zhu, Z. Zheng, S. Xu, Y. He and F. Liu, arXiv preprint arXiv:2005.02689, 2020.